journal

J. Am. Ceram. Soc., 89 [9] 2749–2756 (2006)
DOI: 10.1111/j.1551-2916.2006.01155.x

Synthesis and Characterization of Mixed-Metal Oxide Nanopowders Along the CoO_x–Al_2O_3 Tie Line Using Liquid-Feed Flame Spray Pyrolysis

Jose Azurdia, Julien Marchal, and Richard M. Laine†

Departments of Materials Science and Engineering, and the Macromolecular Science and Engineering Center, University of Michigan, Ann Arbor, Michigan 48109-2136

We report here the use of liquid-feed flame spray pyrolysis (LF-FSP) to produce a series of nanopowders along the CoO_x–Al_2O_3 tie line. The process is a general aerosol combustion synthesis route to a wide range of lightly agglomerated oxide nanopowders. The materials reported here were produced by aerosolizing ethanol solutions of alumatrane [$Al(OCH_2CH_2)_3N$] and a cobalt precursor, made by reacting $Co(NO_3)_2 \cdot 6H_2O$ crystals with propionic acid. The compositions of the as-produced nanopowders were controlled by selecting the appropriate ratios of the precursors. Nine samples with compositions $(CoO)_y(Al_2O_3)_{1-y}$, $y = 0-1$ along the CoO_x–Al_2O_3 tie line were prepared and studied. The resulting nanopowders were characterized by X-ray fluorescence, BET, scanning electron microscopy , high-resolution transmission electron micrographs, X-ray diffraction (XRD), thermogravimetric analysis (TGA), and FTIR. The powders typically consist of single-crystal particles <40 nm diameter and specific surface areas (SSAs) of 20–60 m^2/g. XRD studies show a gradual change in powder patterns from δ-Al_2O_3 to Co_3O_4. The cobalt aluminate spinel phase is observed at stoichiometries (21 and 37 mol%) not seen in published phase diagrams, likely because LF-FSP processing involves a quench of >1000°C in microseconds frequently leading to kinetic rather than thermodynamic products. Likewise, the appearance of Co_3O_4 rather than CoO as the end member in the tie line is thought to be a consequence of the process conditions. TGA studies combined with diffuse reflectance FTIR spectroscopic studies indicate that both physi- and chemi-sorbed H_2O are the principal surface species present in the as-processed nanopowders. The only sample that differs is Co_3O_4, which has some carbonate species present that are detected and confirmed by a sharp mass loss event at ~ 250°C. The thermal behavior of the high cobalt content samples differs greatly from the low cobalt content samples. The latter behave like most LF-FSP-derived nanopowders exhibiting typical 1%–4% mass losses over the 1400°C range due mostly to loss of water and some CO_2. The high cobalt content samples exhibit a sharp mass loss event that can be attributed to the decomposition of Co_3O_4 to CoO.

I. Introduction

Cobalt oxides are used as catalysts for hydrocracking fuels,[1] in several selected and complete oxidation processes,[2,3] as well as in steam reforming of ethanol.[4] Co_3O_4 shows good catalytic activity for the low-temperature combustion of CO and organics.[5] At higher temperatures, the catalyst becomes reducing, converting CO_2 to CO and O_2 without a reducing reagent.[6]

Supported cobalt is often a co-catalyst for hydrocracking waste gases and contaminated fluids[7] to innocuous gases including NO_x. Traditional *de*-NO_x catalysts usually contain one of several very expensive metals including Pd, Pt, Rh, and Ru.[8,9] Supported cobalt systems offer considerable potential as low-cost, selective alternatives for catalytic reduction of NO_x.[10–12]

Cobalt has also been used since prehistoric times as a component in many pigments, particularly for deep blues.[13,14] Typical pigments consist of spinel or olivine phases produced from mixtures of cobalt and SiO_2, ZrO, TiO_2, or Al_2O_3.[15,16] There continues to be considerable active research on cobalt pigment technology to optimize color hues and luminescent properties.[17–19] Cobalt pigments are also used in high-end optical filters and magnetic recording media.[20,21]

The literature is replete with synthetic routes to cobalt oxides, and cobalt-containing materials especially for compositions along the CoO_x–Al_2O_3 tie line. The standard method is via a solid-state reaction of the parent oxides. Other synthesis methods include sol–gel,[22,23] co-precipitation,[24,25] hydrothermal,[26] polymeric precursor,[27] and vapor deposition processing.[28] We demonstrate here the use of liquid-feed flame spray pyrolysis (LF-FSP) to assess combinatorially compositions along the CoO_x–Al_2O_3 tie line. Spray pyrolysis techniques are well known and have been described extensively in the literature: they have been used to synthesize simple and complex oxide powders.[29,30] The advantage of LF-FSP over other techniques is that it allows production of up to 15 different compositions in the time span of a single week and hence can be considered a combinatorial method of synthesizing metal oxide nanopowders.

The LF-FSP process as invented and currently used at University of Michigan,[31] aerosolizes mixtures of metalloorganic compounds (metal carboxylates and/or alkoxides) dissolved in alcohol solvents at known concentration levels using oxygen. The resulting aerosol is ignited via methane pilot torches by combusting the mixture at temperatures between 1500° and 2000°C. The combustion-derived "soot" is collected using wire-in-tube electrostatic precipitators (ESP) as detailed elsewhere.[32] This "soot" consists, normally, of single crystal particles with average particle sizes (APSs) of 10–200 nm depending on processing conditions and corresponding specific surface areas (SSAs) of 100–20 m^2/g. These nanopowders normally have the same composition as that found in the original precursor solution including any inadvertent impurities.

We have previously shown that LF-FSP processing can be used to prepare well-known single metal nanopowders such as alumina (δ-Al_2O_3) and titania (90% anatase, 10% rutile). LF-FSP also provides access to complex mixed-metal oxide materials including mullite, $Y_3Al_5O_{12}$, $SrSi_2Al_2O_8$, and $\beta''Al_2O_3$.[33–35] Because we can control compositional make-up to ppm levels, it is possible to also dope pure materials for photonic, electronic, and catalytic applications.[36,37] In the latter arena, we have recently demonstrated that we can process materials along the

G. Soraru—contributing editor

Manuscript No. 21198. Received November 29, 2005; approved April 7, 2006.
†Author to whom correspondence should be addressed. e-mail: talsdad@umich.edu

TiO_2–Al_2O_3, NiO–Al_2O_3, ZnO–Al_2O_3, and MgO–Al_2O_3 tie lines with the discovery of several unusual phase compositions.[38,39] In this paper, we extend our efforts to develop materials with novel phase compositions of potential interest to the catalyst and pigment industry.

II. Experimental Procedure

(1) Materials

Cobalt nitrate hexahydrate [$Co(NO_3)_2 \cdot 6H_2O$, 99.97%], propionic acid [$CH_3CH_2CO_2H$, 99+%], triethanolamine [$N(CH_2CH_2OH)_3$ 98%], and anhydrous ethanol [CH_3CH_2OH, 99+%] were purchased from Alfa Aesar and used as received. Aluminum tris(sec-butoxide), [$Al(OsBu)_3$, 97%] was purchased from Chattem Chemical Co. and also used as received.

(2) Precursor Formulations

[$Al(OCH_2CH_2)_3N$] was synthesized from $Al(OsBu)_3$ and $N(CH_2CH_2OH)_3$ as described elsewhere,[40] and then diluted with EtOH to produce ~6 L of solution with a ceramic loading of 21 wt% by thermogravimetric analysis (TGA).

Cobalt precursor was prepared by adding 200.0 g (0.687 mole) of $Co(NO_3)_2 \cdot 6H_2O$ crystals to a 500 mL flask equipped with a still head and an N_2 sparge. $CH_3CH_2CO_2H$ (400 mL, 5.36 moles) was added and the resulting solution was heated to ~150°C for 6 h to distill off ~140 mL of liquid (water/$CH_3CH_2CO_2H$) and coincidentally remove NO_x gas. The remaining liquid product was placed in a clean 500 mL Nalgene® bottle. The ceramic loading of the solution was determined by TGA to be 3.3 wt%. We did not further identity this precursor because it is very volatile and coated our TGA instrument, reacting rapidly with any exposed Al_2O_3 forming a cobalt aluminate spinel.

(3) LF-FSP

The LF-FSP system has been described elsewhere in detail.[41] Ethanol precursor solutions were prepared by diluting the sample precursors to a 2–5 wt% ceramic yield, typically 4 wt%. These solutions are then atomized with O_2 through a nozzle. The fine mist generated is ignited with methane–oxygen pilot torches achieving combustion temperatures >1500°C. The products are carried downstream by a radial pressure blower (19.8 m^3/min), and collected downstream in ESP maintained at a 10 kV DC potential. The nanopowders are finally recovered manually from the ESP tubes after the system has cooled down.

(4) Analytical Methods

Chemical analyses were obtained by X-ray fluorescence (XRF) from Ford Motor Company (Dearborn, MI). XRF samples were prepared by mixing 0.50 g of sample in 10.0 g of $Li_2B_4O_7$ glass flux. The sample and glass flux were mechanically stirred for 5 min in a methacrylate vial with three methacrylate balls using an SPEX 6000 ball mill. The mixtures were fused into glass beads by placing them in an oven held at 1000°C for 10 min. The samples were analyzed using a Panalytical PW2400 XRF spectrometer (formerly Philips), equipped with a WDS detection system (wavelength dispersive), by Ford Motor Company personnel.

Surface area analyses were obtained using a Micromeritics ASAP 2010 sorption analyzer (Norcross, GA) for all powders. Samples were loaded (350 mg) and degassed at 350°C until a degas rate of <5 mTorr was achieved, followed by analysis at 77 K with N_2 as the adsorbate gas. The SSAs were calculated using the BET multipoint method. The particles' average diameter was determined by:

$$d = \frac{6}{\rho \times \mathrm{SSA}} \quad (1)$$

where ρ is the theoretical density of the powders and SSA is the specific surface area.

Scanning electron microscopy (SEM) A Philips XL30 SEM (Philips, Eindhoven, the Netherlands) instrument was used to acquire electron micrographs of all samples. The powder samples were first dispersed in 5 mL of DI water using an ultrasonic horn (Vibra-cell, Sonics and Materials Inc., Newton, CT), and next a drop was placed on an SEM sample stub, which was heated on a covered hot plate. The stubs were sputter coated using a Technics Hummer VI sputtering system (Anatech Ltd., Alexandria, VA) to improve resolution.

High-resolution transmission electron micrograph (HR-TEM) images were acquired using a JEOL 4000EX (Osaka, Japan) electron microscope operated at 400 kV. Samples were mounted on a Gatan double-tilt goniometer; they were prepared by dispersing ~5 mg in 5 mL of isopropanol. An ultrasonic water bath at room temperature was used for 5 min to create a homogeneous dispersion. A drop of the dispersion was then placed on a holey carbon film on Cu grids, 300 mesh (SPI Industries, Indianapolis, IN), and placed on a covered hot plate to dry.

X-ray diffraction analysis (XRD) was performed on a Rigaku Rotating Anode Goniometer (Rigaku Denki Co. Ltd., Tokyo, Japan). The powder samples were prepared by packing ~100 mg into in an amorphous silica holder, which were loaded into the machine. Continuous scans were performed from 20° to 80° 2θ, in 0.05° increments at 2°/min. Cu$K\alpha$ radiation (l = 1.54 Å) with a working voltage of 40 kV and a current of 100 mA were used to produce the X-rays. Scan data was analyzed to determine APSs and phases present, using Jade software (Materials Data Inc., Livermore, CA).

Thermogravimetric and differential thermal analysis (TGA–DTA) were performed on an SDT 2960 simultaneous DTA–TGA instrument (TA Instruments Inc., New Castle, DE). Samples were prepared by weighing ~40 mg of powder and pressing it into a pellet (3.0 mm diameter) using a dual action hand press. The samples were placed in an alumina holder and an empty pan was used as a reference. The instrument was ramped 10°C/min up to 1400°C under a continuous flow of 60 mL/min of synthetic air.

Diffuse reflectance infrared fourier transform spectrometry (DRIFTS) for all powders was acquired using a Mattson Galaxy Series FTIR 3000 spectrometer (Mattson Instruments Inc., Madison, WI). Background scans of optical grade KBr were performed by grinding ~400 mg using an alumina mortar and pestle and then packing the powder into a sample holder, and collecting a spectrum. Samples were prepared by adding 4 mg of sample to 400 mg of KBr and grinding them as the background sample. Spectra were collected continuously in the range of 4000–400 cm^{-1} with a scan resolution of ±4 cm^{-1}, with an average of 156 scans. The sample chamber was flushed continuously with N_2 to remove atmospheric CO_2 and moisture.

III. Results and Discussion

We report here the synthesis and characterization of nine nanopowders with compositions along the CoO_x–Al_2O_3 tie line. These materials, produced in a single-step process, offer advantages over more conventionally prepared materials because LF-FSP provides access to phase compositions that are otherwise hard or impossible to attain. This method is extremely versatile, allowing combinatorial alterations of compositions with minimal effort and precise control. Thus, it is possible to produce 40 g samples of 15 different compositions in roughly 5 days or more samples with smaller sample sizes.

All samples exhibit relatively high SSAs, have no microporosity (from T-plot analysis and transmission electron micrographs (TEMs) micrographs), and have spherical morphologies. These and other properties make them excellent candidates for catalytic or pigment applications, both as pure materials and supported on alumina, silica, or other inert oxide support.

Table I. Precursor Compositions

Sample	(Mol%) Co
1	0
2	4
3	8
4	21
5	37
6	50
7	87
8	94
9	100

A discussion on the formulation of the precursors and nanopowder production follows. We then discuss particle morphology in terms of SSAs, shape and size, and surface species using a variety of characterization methods.

(1) Precursor Formulations

Nine different precursor formulations (see Section *II* and Table I) were used to produce nanopowders along the CoO_x–Al_2O_3 tie-line. Precise amounts of $[Al(OCH_2CH_2)_3N]$ and cobalt precursor solutions were diluted with EtOH and stirred mechanically before use for LF-FSP processing. Solutions used to produce the powders contained 2–4 wt% ceramic in precursor form by TGA, to minimize rheological complications with the LF-FSP process. The compositions produced are listed in Table I. We produced 40 g samples of all powders at 30–100 g/h rates. XRF was used to obtain elemental analyses of selected samples, and the results showed that the compositions were within experimental error of the precursor compositions.

(2) Powder Characterization

SSAs of all as-produced samples are shown in Fig. 1. The SSAs clearly decrease toward the CoO_x-rich end of the tie line, with the exception of the Co_3O_4 powder. The decrease appears coincident with the formation of cobalt spinel phase as Co^{3+} ions are incorporated into the Al_2O_3 matrix. The increase in surface area of the last sample results from oxidation of CoO to Co_3O_4, which causes a phase change coincident with a change in density, leading to an intrinsic increase in SSA. No microporosity was expected nor detected in any of the samples.

The APSs were estimated from the SSAs and the theoretical density of the powders, and compared with values obtained by Debye–Scherrer XRD peak-broadening analyses. The theoretical density values where computed using the known values of the end members and middle composition of the tie line, (Al_2O_3, $CoAl_2O_4$, and Co_3O_4) and interpolating using compositions in mole percent for the various samples. Particle sizes obtained by Debye–Scherrer peak broadening differ somewhat from those calculated from BET calculations (see Table II).

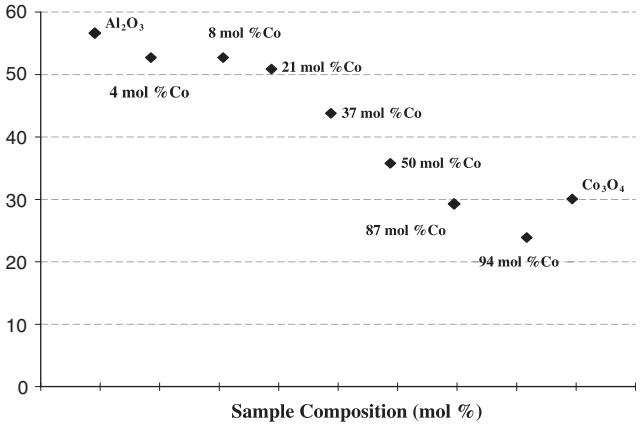

Fig. 1. Specific surface areas (SSAs) of all powder samples. SSAs are ± 2 m^2/g.

Table II. Average Particle Sizes (APS) from BET and XRD Data

Sample	(Mol%) Co	BET APS (nm)	XRD APS (nm)
1	Al_2O_3	29	29
2	4	31	18
3	8	30	21
4	21	30	20
5	37	32	19
6	50	38	22
7	87	35	21
8	94	40	22
9	100	32	20

XRD, X-ray diffraction.

The APS values from peak-broadening technique are lower by $\sim$10–20 nm; this is possibly due to a difference in actual versus theoretical densities of the powder, except for the value of pure Al_2O_3, which corresponds well with the value calculated from the SSA. The APS of all powders is $<$40 nm regardless of the technique used to calculate the value, and remains relatively constant for all compositions studied.

Scanning electron micrographs (SEMs) of all samples provided an understanding of particle morphology. Figure 2 shows SEMs of the 21 and 50 mol% Co samples, which are representative of all other samples. The powders exhibit spherical morphologies throughout and the images suggest relatively narrow particle size distributions. The SEMs show a few particles in the 100–150 nm range and some agglomerates formed via electrostatic interactions. Figure 2(b) was taken at low magnification to

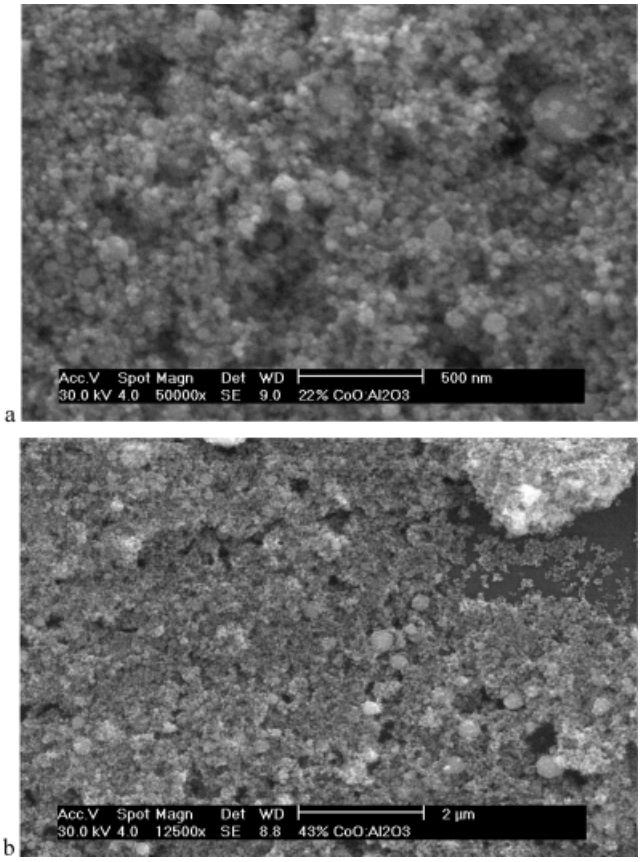

Fig. 2. SEMs showing homogenous spherical morphology and narrow particle distribution.

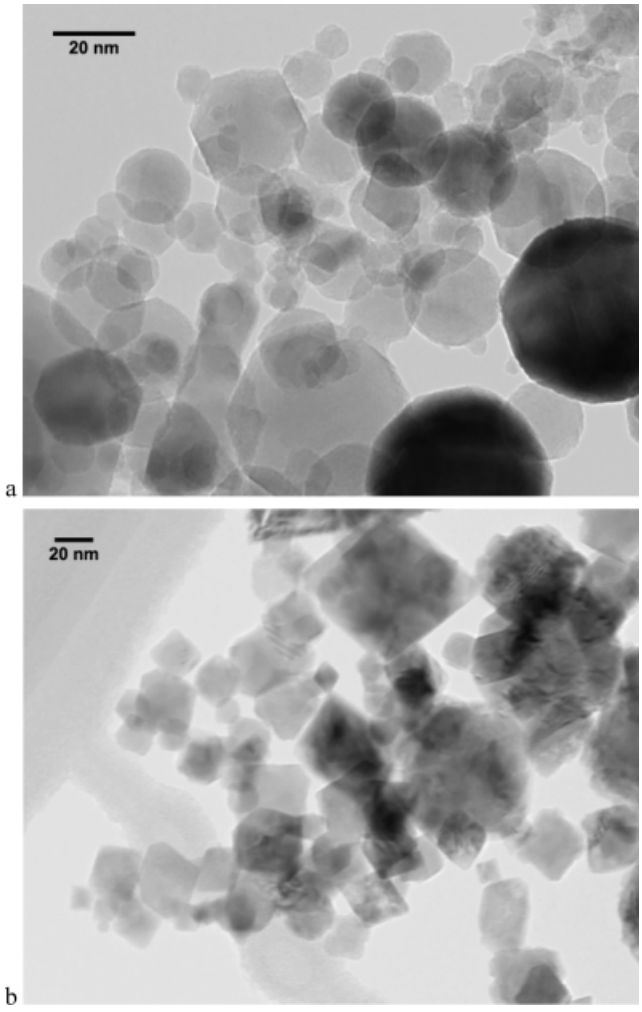

Fig. 3. Transmission electron micrographs of 8 and 87 mol% Co samples. Note the change in particle morphology.

provide an overview of the general particle population that allows one to conclude that no micron size particles are produced during LF-FSP of these materials.

TEMs are shown in Fig. 3. These images are, respectively, from the 8 and 87 mol% Co samples. Most of the particles are spherical and well below 80 nm in diameter, with the vast majority <30 nm. Note the change in morphology, which is mostly faceted and spherical for the 8 mol% sample (Fig. 3(a)), while nearly all particles in the 87 mol% sample (Fig. 3(b)) appear rhombic. This is attributed to the formation of the highly crystalline spinel phase coincident with increases in Co content. Particle necks, while occasionally visible in the 8 mol% sample, are not a major morphological feature. All samples prepared here consist primarily of soft agglomerates created during dispersion or from the strong electrostatic interactions that particles of this size exhibit. There is no evidence for any microporosity, as expected from the *t*-plot results and analyses.

XRDs for all samples are presented in Fig. 4. Figure 5 shows the relevant ICDD cards (CoO:43-1004, Co_3O_4:42-1467, $CoAl_2O_4$:44-0160, δ-Al_2O_3:46-1131, δ^*-Al_2O_3:46-1215). The phase composition changes gradually from δ-Al_2O_3 through the spinel phase to Co_3O_4.

The 4 mol% Co sample shows no trace of any Co-containing crystalline phase; thus, all of the Co^{3+} seems to substitute for Al^{3+} ions in the δ-Al_2O_3 lattice as expected based on our studies on rare-earth-doped δ-Al_2O_3.[41]

Samples with higher Co contents exhibit powder patterns corresponding to formation of $CoAl_2O_4$ spinel. These broad peaks first appear at 21 mol% Co and give way to sharper, better-defined peaks as the correct stoichiometry is reached. Stoichiometric cobalt aluminate shows a phase-pure pattern (ICDD ref.: 44-0160), indicative of the capabilities of LF-FSP. Figure 5 shows the compositions and the phases that are expected to form at these compositions. The formation of off-stoichiometric spinels (21 and 37 mol% samples) is believed to result from the extremely fast quench that these materials undergo in the LF-FSP apparatus. The shifts in the peak positions are indicative of a change in lattice cell parameters; however, in order to determine the exact atom positions in these materials, further studies are required.

In the 87 mol% Co sample, a CoO phase is detected as the excess Co^{3+} ions have no more sites to replace in the spinel structure. This phase is evident by a shift to higher $2\theta^\circ$($\sim 0.8\theta^\circ$) in the 220 reflection, and the emergence of a shoulder on the 400 reflection of $CoAl_2O_4$ and Co_3O_4. In the 94 mol% sample, the CoO phase is clearly evidenced by the emergence of the CoO 200 reflection ($\sim 42^\circ$ 2θ) and the 220 reflection ($\sim 62^\circ$ 2θ) Fig. 6.

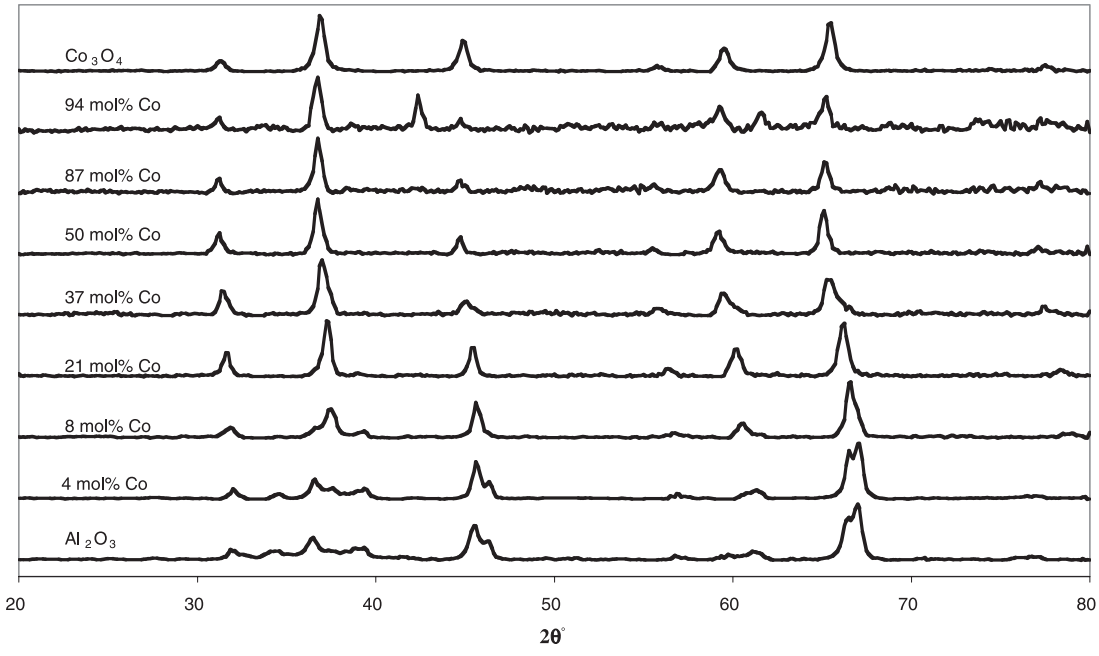

Fig. 4. X-ray diffraction of all as-prepared samples.

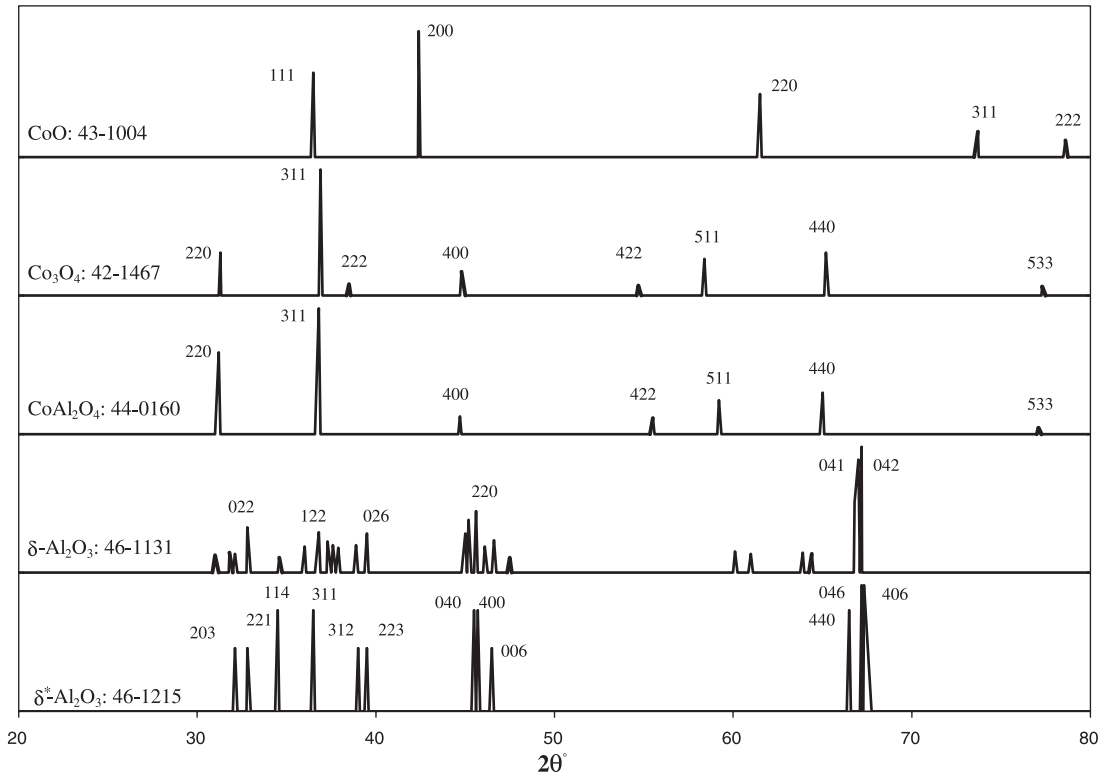

Fig. 5. Relevant ICDD files for the CoO_x–Al_2O_3 system.

The 94 mol% Co sample consists of a mixture of two phases, spinel $CoAl_2O_4$ and cubic CoO, as expected based on the elemental composition and the phase diagram.[42] The pure cobalt oxide XRD corresponds to Co_3O_4, which has a spinel structure from the ICDD card. We do not observe the thermodynamically expected cubic CoO because LF-FSP syntheses use O_2-rich atmospheres. The excess oxygen favors the formation of Co^{3+}, which in turn favors the formation of the spinel [Co_1(II)-Co_2(III)O_4] structure, detected by XRD.

TGA were performed on all as-prepared samples to determine the relative amounts of adsorbed surface species (H_2O and carbonate species) and thermal behavior. The 87, 94 mol% Co and Co_3O_4 show no mass loss events below ~900°C. At this temperature, these materials exhibit a sharp mass loss event that can be attributed to decomposition from Co_3O_4 to CoO:

$$2Co_3O_4 \rightarrow 6CoO + O_2 \quad (2)$$

The theoretical mass loss for such a reaction is 6.64%; the observed losses are 6.13, 6.02, and 6.09, respectively, for the 87, 94 mol% Co and Co_3O_4. These values are within the

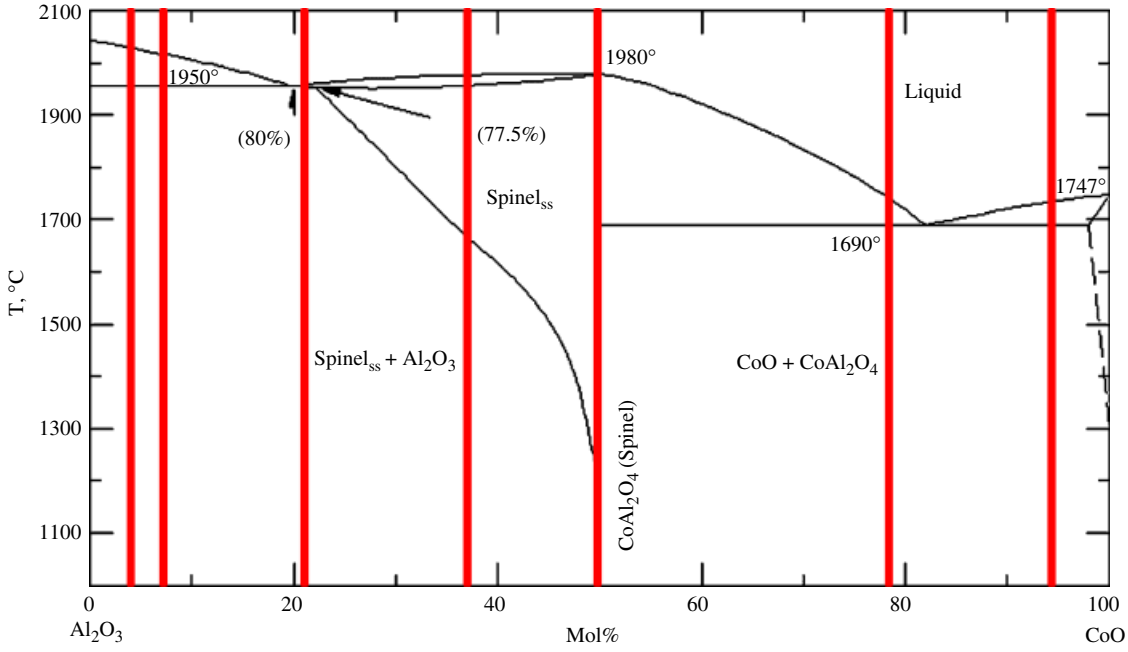

Fig. 6. Published phase field diagram for the CoO–Al_2O_3 system.[42]

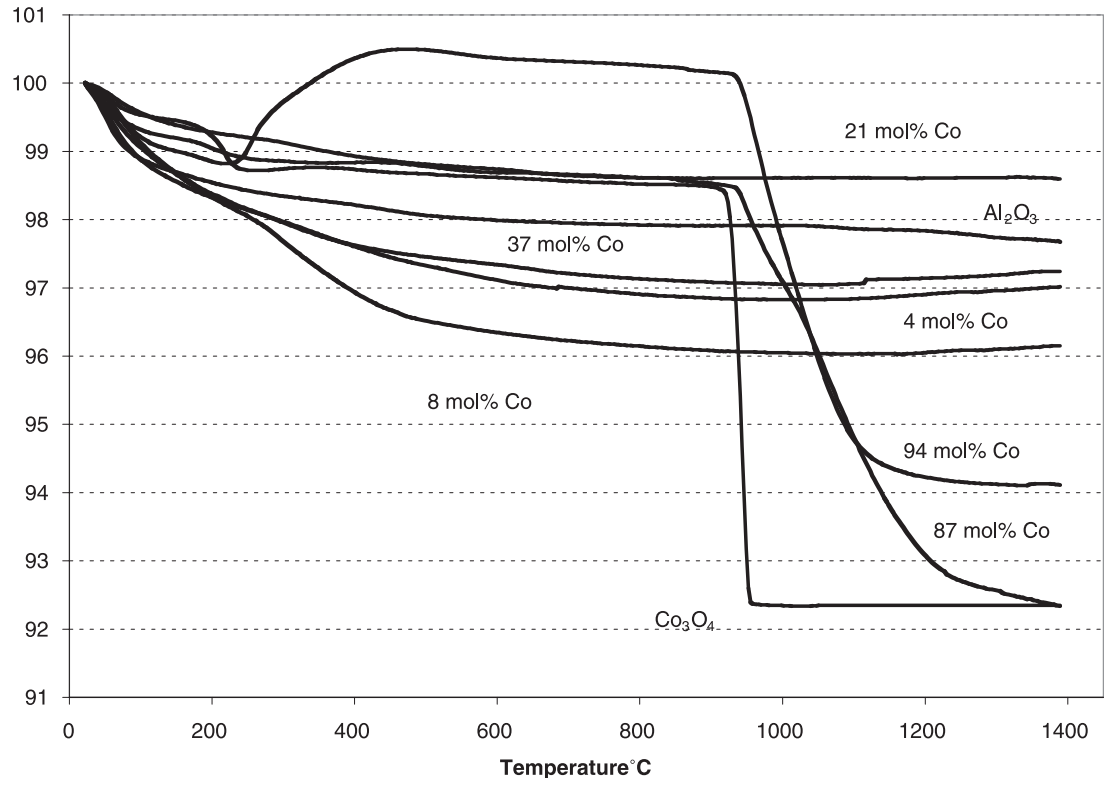

Fig. 7. Thermal behavior (10°C/min, 60 mL/min in air) for all as-prepared samples.

error limits of the analysis, given that these samples contain some CoO (see XRD analyses). The Co_3O_4 end member exhibits the sharpest mass loss event, which is observed to broaden at lower Co contents. One possible explanation is that oxygen is more tightly bound to nanopowders with some $CoAl_2O_4$ spinel phase present, although this was not confirmed here.

There is a small mass increase (0.5 wt%) between 240° and 450°C in the 94 mol% Co sample; we suspect that this increase results from oxidation of some CoO to Co_3O_4 or cobalt spinel. Such an oxidation might be expected for Co^{2+} ions substituted for octahedral Co^{3+} ions in the as-prepared material. These ions occupy traditional "B" sites in spinels that require a 3^+ charge to be stoichiometric.

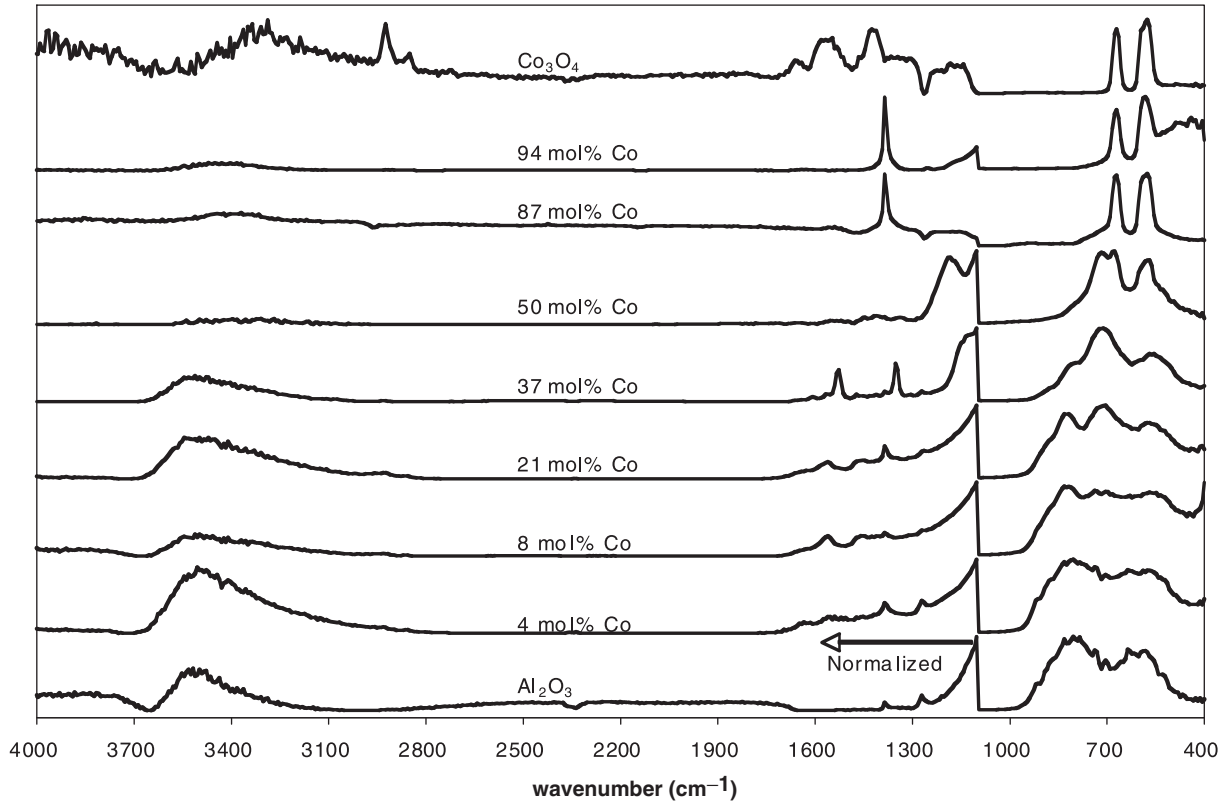

Fig. 8. Full FTIR spectra of all as-prepared samples.

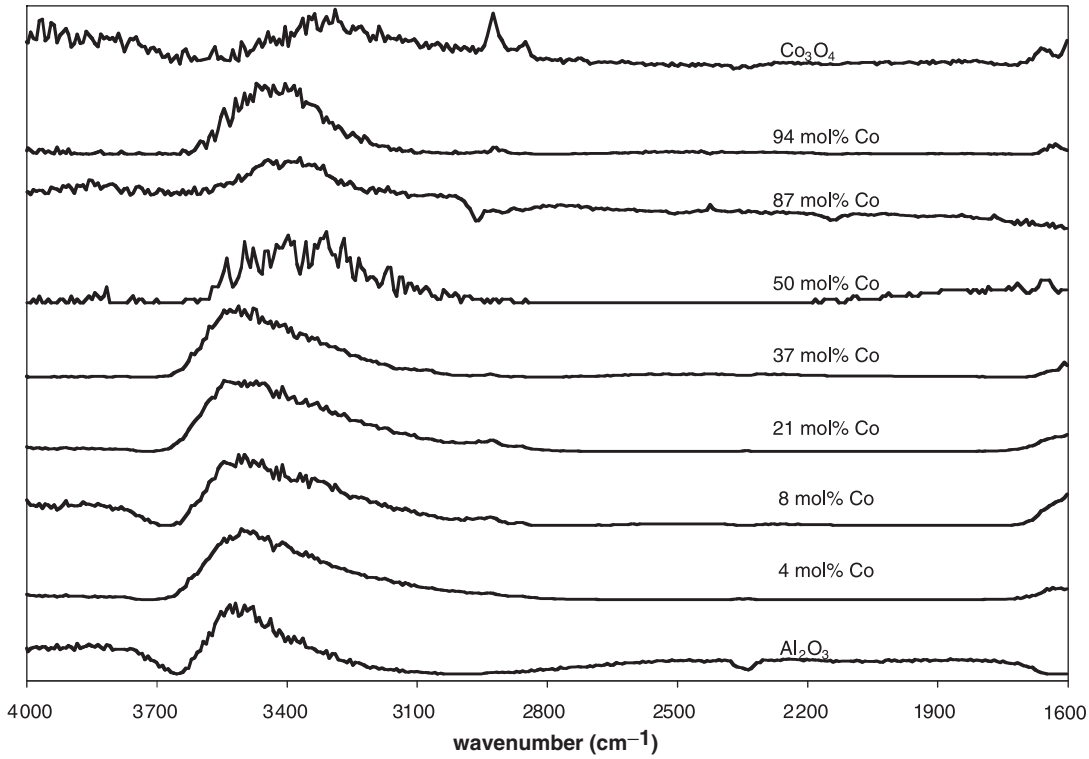

Fig. 9. FTIR spectra of all normalized samples in the 4000–1600 cm^{-1} region.

The other five samples exhibit typical 1%–4% mass losses (for nanopowders produced via LF-FSP) over the 1400°C range. This loss is expected and associated with loss of physi- and chemi-sorbed water resulting from the combustion process and atmosphere due to their relatively high surface areas, although they exhibit far less hydration than microporous powders.[43] The only sample that has a sharp mass loss event is Co_3O_4 at ~250°C; this event can be associated with loss of CO_2 or CO_3^{2-}.[33] DRIFTS data (discussed below) confirm the presence of organics.

DRIFTS for all samples are presented in Fig. 8. All spectra above 1200 cm^{-1} were normalized by taking the highest count in this range of any particular spectrum and normalizing this value to 1; this was done so that a fair comparison can be made among all spectra.

There are two main regions of interest: 4000–2800 and 1100–400 cm^{-1}. The first region, expanded in Fig. 9, reveals a series of overlapping ν–OH bands arising from both physi- and chemisorbed water. The higher ν–OH vibrations (3700–3200 cm^{-1}) are typical of overlapping hydroxyl groups on alumina surfaces.[44,45] There are no sharp peaks in this region, only broad bands. Furthermore, the νO–H bands fall off with increases in Co content, suggesting that the surface hydroxyls are only associated with the alumina species. With the exception of Co_3O_4, no significant organic species are observed as evidenced by the absence of νC–H bands in the 2900–2700 cm^{-1} region. These bands are associated with a 2% mass loss seen at >250°C in the TGA trace and could be a result of incomplete combustion of the precursor. However, this seems unlikely as they are not normally observed in any other nanopowders prepared previously and may be better explained as resulting from some steam reforming in the flame. But this conclusion remains speculative.

The lower wavenumber region exhibits typical νM–O bands. δ-alumina has two νAl–O bands at 810 and 610 cm^{-1},[46] associated with the tetrahedral and octahedral Al–O vibrations, respectively. Cobalt oxide (Co_3O_4) has two well-defined νM–O bands, 690 and 605 cm^{-1},[47] which emerge clearly in the higher Co content samples. These sharp bands become visible in sample 7:87 mol% Co, and are associated with the high degree of crystallinity of these samples.

IV. Conclusions

LF-FSP offers the opportunity to produce mixed-metal oxide nanopowders with exceptional control of stoichiometry, phase, and phase purity. Here, we demonstrate the use of LF-FSP to produce combinatorially a series of nine powders along the CoO_x–Al_2O_3 tie line with well-defined stoichiometries. The precursors used to synthesize these nanopowders are inexpensive and can be easily prepared.

We find that along the CoO_x–Al_2O_3 tie line, increases in Co content steadily reduce the SSAs by as much as 65% (from 60 to 20 m^2/g), likely as a consequence of the formation of the cobalt spinel phase. Particle sizes (from XRD data) vary very little; the BET-derived APS values are slightly higher most likely because of miscalculations in the true particle densities. The unexpected SSA increase observed for the end-member cobalt oxide is attributed to the formation of Co_3O_4 instead of CoO. The most probable explanation for this result is that the excess oxygen used in the LF-FSP process favors formation of Co^{3+}, which in turn favors the formation of a spinel [Co_1(II)Co_2(III)O_4] structure. We also detected cobalt aluminate spinel phases that should only be stable at high temperatures, but found they were metastable at lower temperatures. Therefore we can conclude that LF-FSP offers access to kinetic phases rather than the thermodynamic phases accessible by standard processing techniques.

For the most part, TGA and FTIR studies provide results that correspond to typical nanopowders produced via LF-FSP. These materials exhibit typical 1%–4% mass losses over the 1400°C range, with only physi- and chemisorbed water as a surface species. Carbonate species, often detected on the surfaces of LF-FSP powders, here Co_3O_4, yield mass loss events at ~250°C attributed to elimination of CO_2. The sharp mass loss event of the high cobalt content samples likely results from decomposition of Co_3O_4 to CoO but is at present only speculation.

References

[1]S. Ucar, S. Karagoz, T. Karayildirim, and J. Yanik, "Conversion of Polymers to Fuels in a Refinery Stream," *Polym. Degrad. Stabil.*, **75**, 161–71 (2002).

[2]J. Rodriguez, C. Guimon, A. J. Marchi, A. Borgna, and A. Monzon, "Activity, Selectivity and Coking of Bimetallic Ni–Co-Spinel Catalysts in Selective Hydrogenation Reactions," *Stud. Surf. Sci. Catal.*, **111**, 183–90 (1997).

[3]P. Thormahlen, E. Fridell, N. Cruise, M. Skoglundh, and A. Palmqvist, "The Influence of CO_2, C_3H_6, NO, H_2, H_2O or SO_2 on the Low-Temperature Oxidation of CO on a Cobalt–Aluminate Spinel Catalyst ($Co_{1.66}Al_{1.34}O_4$)," *Appl. Catal. B-Environ.*, **31** [1] 1–12 (2001).

[4]J. Llorca, P. D. Ramırez De La Piscina, J.-A. Dalmon, and N. Homs, "Transformation of Co_3O_4 During Ethanol Steam-Re-Forming. Activation Process for Hydrogen Production," *Chem. Mater.*, **16**, 3573–8 (2004).

[5]F. Grillo, M. M. Natile, and A. Glisenti, "Low Temperature Oxidation of Carbon Monoxide: The Influence of Water and Oxygen on the Reactivity of a Co_3O_4 Powder Surface," *Appl. Catal. B-Environ.*, **48**, 267–74 (2004).

[6]L. B. Backman, A. Rautiainen, M. Lindblad, and A. O. I. Krause, "Effect of Support and Calcination on the Properties of Cobalt Catalysts Prepared by Gas Phase Deposition," *Appl. Catal. A-Gen.*, **191** [1–2] 55–68 (2000).

[7]S. Karagoz, T. Karayildirim, S. Ucar, M. Yukselc, and J. Yanikb, "Liquefaction of Municipal Waste Plastics in VGO Over Acidic and Non-Acidic Catalysts," *Fuel*, **82**, 415–23 (2003).

[8]A. Hadi and I. Yaacob, "Synthesis of PdO/CeO_2 Mixed Oxides Catalyst for Automotive Exhaust Emissions Control," *Catal. Today*, **96** [3] 165–70 (2004).

[9]T. Kanazawa, "Development of Hydrocarbon Adsorbents, Oxygen Storage Materials for Three-Way Catalysts and NO_x Storage-Reduction Catalyst," *Catal. Today*, **96** [3] 171–7 (2004).

[10]M. Richter, M. Langpape, S. Kolf, G. Grubert, R. Eckelt, J. Radnik, M. Schneider, M. M. Pohl, and R. Fricke, "Combinatorial Preparation and High-Throughput Catalytic Tests of Multi-Component deNO_x Catalysts," *Appl. Catal. B-Environ.*, **36** [4] 261–77 (2002).

[11]S. Matsumoto, "Recent Advances in Automobile Exhaust Catalysts," *Catal. Today*, **90** [3–4] 183–90 (2004).

[12]J. Li, J. Hao, L. Fu, T. Zhu, Z. Liu, and X. Cui, "Cooperation of Pt/Al_2O_3 and In/Al_2O_3 Catalysts for NO Reduction by Propene in Lean Burn Condition," *Appl. Catal. A-Gen.*, **265** [1] 43–52 (2004).

[13]P. Colomban, "Lapis Lazuli as Unexpected Blue Pigment in Iranian Lajvardina Ceramics," *J. Raman Spectrosc.*, **34** [6] 420–3 (2003).

[14]C. Roldan, J. Coll, J. L. Ferrero, and D. Juanes, "Identification of Overglaze and Underglaze Cobalt Decoration of Ceramics from Valencia (Spain) by Portable EDXRF Spectrometry," *X-ray Spectrom.*, **33** [1] 28–32 (2004).

[15]L. Koroleva, "Synthesis of Spinel-Based Ceramic Pigments from Hydroxycarbonates," *Glass Ceram.*, **61** [9–10] 299–302 (2004).

[16]S. Djambazov, Y. Ivanova, A. Yoleva, and N. Nedelchev, "Ceramic Pigments on the Base of the CoO–ZnO-SiO_2 System Obtained by a Sol–Gel Method," *Ceram. Int.*, **24** [4] 281–4 (1998).

[17]J. Merikhi, H.-O. Jungk, and C. Feldmann, "Sub-Micrometer $CoAl_2O_4$ Pigment Particles—Synthesis and Preparation of Coatings," *J. Mater. Chem.*, **10**, 1211–314 (2000).

[18]T. Junru, H. Yunfang, H. Wenxiang, C. Xiuzeng, and F. Xiansong, "The Preparation and Characteristics of Cobalt Blue Mica Coated Titania Pearlescent Pigment," *Dyes Pigm.*, **52** [3] 215–22 (2002).

[19]M. Llusar, A. Fores, J. A. Badenes, J. Calbo, M. A. Tena, and G. Monros, "Colour Analysis of Some Cobalt-Based Blue Pigments," *J. Eur. Ceram. Soc.*, **21** [8] 1121–30 (2001).

[20]Z.-Z. Chen, E.-W. Shi, W.-J. Li, Y.-Q. Zheng, and W.-Z. Zhong, "Hydrothermal Synthesis and Optical Property of Nano-Sized $CoAl_2O_4$ Pigment," *Mater. Lett.*, **55** [5] 281–4 (2002).

[21]M. P. Morales, S. A. Walton, L. S. Prichard, C. J. Serna, D. P. E. Dickson, and K. O'grady, "Characterisation of Advanced Metal Particle Recording Media Pigments," *J. Magn. Magn. Mater.*, **190**, 357–70 (1998).

[22]C. O. Arean, M. P. Mentruit, E. E. Platero, F. X. L. I. Xamena, and J. B. Parra, "Sol–Gel Method for Preparing High Surface Area $CoAl_2O_4$ and Al_2O_3–$CoAl_2O_4$ Spinels," *Mater. Lett.*, **39**, 22–7 (1999).

[23]F. Meyer, A. Dierstein, C. Beck, W. Hartl, R. Hempelmann, S. Mathur, and M. Veith, "Size-Controlled Synthesis of Nanoscaled Aluminium Spinels Using Heterobimetallic Alkoxide Precursors Via Water/Oil Microemulsions," *Nanostruct. Mater.*, **12**, 71–4 (1999).

[24]N. Ouahdi, S. Guillemet, J. J. Demai, B. Durand, L. Er Rakho, R. Moussa, and A. Samdi, "Investigation of the Reactivity of $AlCl_3$ and $CoCl_2$ Toward Molten Alkali-Metal Nitrates in Order to Synthesize $CoAl_2O_4$," *Mater. Lett.*, **59** [2–3] 334–40 (2005).

[25]S. Chokkaram, R. Srinivasan, D. R. Milburn, and B. H. Davis, "Conversion of 2-Octanol Over Nickel–Alumina, Cobalt–Alumina, and Alumina Catalysts," *J. Mol. Catal. A-Chem.*, **121**, 157–69 (1997).

[26]Z.-Z. Chen, E. W. Shi, W.-J. Li, Y.-Q. Zheng, J.-Y. Zhuang, B. Xiao, and L.-A. Tang, "Preparation of Nanosized Cobalt Aluminate Powders by a Hydrothermal Method," *Mater. Sci. Eng. B-Solid*, **107**, 217–23 (2004).

[27]W.-S. Cho and M. Kakihana, "Crystallization of Ceramic Pigment $CoAl_2O_4$ Nanocrystals From Co–Al Metal Organic Precursor," *J. Alloy Compounds*, **287** [1–2] 87–90 (1999).

[28]V. Dureuil, C. Ricolleau, M. Gandais, C. Grigis, J. P. Lacharme, and A. Naudon, "Growth and Morphology of Cobalt Nanoparticles on Alumina," *J. Cryst. Growth*, **233**, 737–48 (2001).

[29]a. W. Stark, L. Madler, M. Maciejewski, S. Pratsinis, and A. Baiker, "Flame Synthesis of Nanocrystalline Ceria–Zirconia: Effect of Carrier Liquid," *Chem. Commun.*, [5] 588–9 (2003). b. A. Camenzind, R. Strobel, and S. E. Pratsinis, "Cubic or Monoclinic Y_2O_3:Eu^{3+} Nanoparticles by One Step Flame Spray Pyrolysis," *Chem. Phys. Lett.*, **415**, 193–7 (2005). c. R. Mueller, R. Jossen, H. K. Kammler, S. E. Pratsinis, and M. K. Akhtar, "Growth of Zirconia Particles Made by Flame Spray Pyrolysis," *J. AIChE*, **50**, 3085–94 (2004). d. R. Mueller, R. Jossen, S. E. Pratsinis, M. Watson, and M. K. Akhtar, "Zirconia Nanoparticles Made in Spray Flames at High Production Rates," *J. Am. Ceram. Soc.*, **87**, 197–202 (2004).

[30]L. S. Wang, Y. H. Zhou, Z. W. Quan, and J. Lin, "Formation Mechanisms and Morphology Dependent Luminescence Properties of Y_2O_3: Eu Phosphors Prepared by Spray Pyrolysis Process," *Mater. Lett.*, **59** [10] 1130–3 (2005).

[31]a. R. M. Laine, K. Waldner, C. Bickmore, and D. R. Treadwell, "Ultrafine Powders by Flame Spray Pyrolysis," U.S. patent 5,958,361, September 28, 1999. b. R. M. Laine, S. C. Rand, T. Hinklin, and G. Williams, "Ultrafine Powders as Lasing Media," International patent application allowed. WO 0038282 H01S 20000629. c. A. C. Sutorik, R. M. Laine, J. Marchal, T. Johns, and T. Hinklin, "Mixed-Metal Oxide Particles by Liquid Feed-Flame Spray Pyrolysis of Oxide Precursors in Oxygenated Solvents," WO03070640 issued 2003-08-28. U.S. Patent issued.

[32]C. R. Bickmore, K. F. Waldner, D. R. Treadwell, and R. M. Laine, "Ultrafine Spinel Powders by Flame Spray Pyrolysis of a Magnesium Aluminum Double Alkoxide," *J. Am. Ceram. Soc.*, **79** [5] 1419–23 (1996).

[33]J. Marchal, T. John, R. Baranwal, T. Hinklin, and R. M. Laine, "Yttrium Aluminum Garnet Nanopowders Produced by Liquid-Feed Flame Spray Pyrolysis (LF-FSP) of Metalloorganic Precursors," *Chem. Mater.*, **16** [5] 822–31 (2004).

[34]D. R. Treadwell, A. C. Sutorik, S. S. Neo, R. M. Laine, and R. Svedberg, "Synthesis of Beta″-Alumina Polymer Precursor and Ultrafine Beta″–Alumina Composition Powders," *Acs. Sym. Ser.*, **681**, 146–56 (1998).

[35]R. Baranwal, M. P. Villar, R. Garcia, and R. M. Laine, "Flame Spray Pyrolysis of Precursors as a Route to Nano-Mullite Powder: Powder Characterization and Sintering Behavior," *J. Am. Ceram. Soc.*, **84** [5] 951–61 (2001).

[36]S. M. Redmond, G. L. Armstrong, H. Y. Chan, E. Mattson, A. Mock, B. Li, J. R. Potts, M. Cui, S. C. Rand, S. L. Oliveira, J. Marchal, T. Hinklin, and R. M. Laine, "Electrical Generation of Stationary Light in Random Scattering Media," *J. Opt. Soc. Am. B*, **21** [1] 214–22 (2004).

[37]G. R. Williams, S. B. Bayram, S. C. Rand, T. Hinklin, and R. M. Laine, "Laser Action in Strongly Scattering Rare-Earth-Metal-Doped Dielectric Nanophosphors," *Phys. Rev. A*, **65** [1] 13807–12 (2002).

[38]S. Kim, J. J. Gislason, R. W. Morton, X. Q. Pan, H. P. Sun, and R. M. Laine, "Liquid-Feed Flame Spray Pyrolysis of Nanopowders in the Alumina–Titania System," *Chem. Mater.*, **16** [12] 2336–43 (2004).

[39]J. Azurdia, J. C. Marchal, P. Shea, H. Sun, X. Q. Pan, and R. M. Laine, "Liquid-Feed Flame Spray Pyrolysis (LF-FSP) as a Method of Producing Mixed-Metal Oxide Nanopowders of Potential Interest as Catalytic Materials. Nanopowders Along the NiO–Al_2O_3 Tie-Line Including $(NiO)_{0.22}(Al_2O_3)_{0.78}$, A New Inverse Spinel Composition," *Chem. Mater.*, **18** [3] 731–9 (2006).

[40]K. F. Waldner, R. M. Laine, S. Dhumrongvaraporn, S. Tayaniphan, and R. Narayanan, "Synthesis of a Double Alkoxide Precursor to Spinel ($MgAl_2O_4$) Directly from $Al(OH)_3$, MgO, and Triethanolamine and its Pyrolytic Transformation to Spinel," *Chem. Mater.*, **8** [12] 2850–7 (1996).

[41]T. Hinklin, B. Toury, C. Gervais, F. Babonneau, J. J. Gislason, R. W. Morton, and R. M. Laine, "Liquid-Feed Flame Spray Pyrolysis of Metalloorganic and Inorganic Alumina Sources in the Production of Nanoalumina Powders," *Chem. Mater.*, **16** [1] 21–30 (2004).

[42]T. Mori, "Phase Diagram of the System Cobalt(II) Oxide–Aluminum Oxide," *Nippon. Seram. Kyokai. Gakkaishi*, **90** [2] 100–1 (1982).

[43]J. M. Mchale, A. Navrotsky, and A. J. Perrotta, "Effects of Increased Surface Area and Chemisorbed H_2O on the Relative Stability of Nanocrystalline -Al_2O_3 and -Al_2O_3," *J. Phys. Chem. B*, **101** [4] 603–13 (1997).

[44]D. H. Lee and S. Condrate, "An FTIR Spectral Investigation of the Structural Species Found on Alumina Surfaces," *Mater. Lett.*, **23** [4–6] 241–6 (1995).

[45]J. M. Saniger, "Al–O Infrared Vibrational Frequencies of [Gamma]-Alumina," *Mater. Lett.*, **22** [1–2] 109–13 (1995).

[46]P. Tarte, "Infra-Red Spectra of Inorganic Aluminates and Characteristic Vibrational Frequencies of AlO_4 Tetrahedra and AlO_6 Octahedra," *Spectrochim. Acta A-M*, **23** [7] 2127–43 (1967).

[47]P. Nkeng, J.-F. Koenig, J. L. Gautier, P. Chartier, and G. Poillerat, "Enhancement of Surface Areas of Co_3O_4 and $NiCo_2O_4$ Electrocatalysts Prepared by Spray Pyrolysis," *J. Electroanal. Chem.*, **402**, 81–9 (1996). □